

## Template-based fabrication of nanoporous metals

Thomas A. Rebbecchi Jr. and Ying Chen<sup>a)</sup>

*Department of Materials Science and Engineering, Rensselaer Polytechnic Institute, Troy, New York 12180, USA*

(Received 8 May 2017; accepted 5 September 2017)

Nanoporous metallic foams with high surface area and novel functional behavior are positioned to stimulate new multifunctional and metamaterial applications. However, there are fundamental challenges in achieving uniform nanopores and tailorable morphology. Emerging templating methods offer a wide range of applicable metallic species while enhancing control of pore morphology, uniformity, and interconnectivity. Here, a critical review of nanoporous metal fabrication is presented, with focus on templating methods utilizing nanoporous polymeric templates. Metals are introduced into percolative nanochannels of sacrificial templates by deposition, and subsequent removal of templates yields ordered nanoporous metals. We introduce approaches for preparing nanoporous templates, including utilizing block copolymer self-assembly that yields periodic gyroid networks. While metallization of templates by electrodeposition has been demonstrated, electroless deposition permits uniform deposition by many metallic species and infiltration of narrow pores. Examples of nanoporous metals with uniform pore sizes below 50 nm fabricated by templating methods are examined.



Ying Chen

Ying Chen received her Ph.D. in Materials Science and Engineering from Massachusetts Institute of Technology in 2008, and her B.S. in Materials Science and Engineering from Tsinghua University in 2004. Her doctoral research dealt with topological percolation effects in heterogeneous material systems (such as grain boundary networks and multiphase materials) and prediction of effective properties. She was a postdoctoral associate at MIT from 2008 to 2010, working on superelastic alloys for armor applications at the Institute for Soldier Nanotechnologies. She then worked as a materials scientist in the Structural and Functional Metals Laboratory at GE Global Research Center in Niskayuna, NY for over a year. While at GE she worked on fatigue and creep properties of polycrystalline superalloys for high temperature applications. She is currently an assistant professor in the Department of Materials Science and Engineering at Rensselaer Polytechnic Institute, Troy, NY, USA. Her research primarily focuses on elucidating microstructure-mechanical property relationships in metallic materials using both experimental and mesoscale modeling approaches. Her current research interests include nanostructured metals, shape memory materials, interface engineering, microstructure design, and mechanical properties. She is an active member of Materials Research Society and has recently co-organized two MRS symposia on metals in extreme conditions and interfaces, respectively.

### I. INTRODUCTION

Nanoporous metals (NPMs) containing a network of nanoscale pores provide an attractive combination of physical and mechanical properties afforded to them by their nanostructures. Offering low density, high specific (i.e., density-normalized) surface area, and high specific strength while retaining many characteristics of bulk metals, this burgeoning class of metallic materials has garnered considerable research interest.<sup>1–6</sup> In addition to use as lightweight materials, nanoporous metals also have potential applications in a diverse array of technologies, such as optical metamaterial,<sup>7</sup> catalysis,<sup>8,9</sup> energy storage,<sup>10</sup> gas storage and filtration,<sup>11</sup>

electromagnetic sensing,<sup>12</sup> and high-coercivity magnets.<sup>2</sup> With the continued realization of their unique properties, nanoporous metals are positioned to drastically invigorate the applicability of metals in new high-performance applications. However, challenges in synthesis of nanoporous metallic materials continue to limit the extent to which they are understood.

The synthesis of highly ordered, nanostructured porous metallic materials represents an important area of contemporary exploration. While methods for the fabrication of nanoporous metals have proliferated over the last two decades, many yield metals with inhomogeneous pore dimensions and are not generalizable to a large majority of metallic species. Table I summarizes several common methods for fabricating porous metals and details their corresponding pore characteristics. While additional methods exist for the creation of nanoporous oxides, the prime focus of this review is

Contributing Editor: Paolo Colombo

<sup>a)</sup>Address all correspondence to this author.

e-mail: chen20@rpi.edu

DOI: 10.1557/jmr.2017.383

TABLE I. A survey of methods that are commonly used for fabricating nanoporous metals.

Fabrication						
Type	Method	Metal	Pore size $d$ (nm)	Pore size distribution	Pore morphology	Porosity depth ( $\mu\text{m}$ )
Chemical	Dealloying	Au <sup>3,5,15,16,18,71–79</sup>	5–200	Alloy dependent	Random orientation with ligament-pore continuity	1000+
		Ag <sup>5,18,80–84</sup>	30–450	Alloy dependent		900+
		Pt <sup>5,80,85</sup>	3.5–100	...		200
		Pd <sup>5,17,80,86–89</sup>	3–25	Al <sub>3</sub> Pd homogeneous, Al <sub>3</sub> Pd <sub>2</sub> not susceptible		...
	Combustion	Ni <sup>19,95–98</sup>	41 ± 25, 71 ± 45	Heterogeneous	Random, bicontinuous mesopore ligands containing nanopores	1.1
		Cu <sup>20,90–94</sup>	25–100	Method dependent		50
Electrodeposition	Fe, Cu, Ag, Co <sup>4,6</sup>	20–200, 1000–3000	Bimodal	Uniformly oriented cylinders	25,000+	
Thermo-mechanical	Sintering	Cu, Sn <sup>25,26</sup>	50–25,000	$d$ increases with distance from substrate	450	
		Ti, steel <sup>27,28,69,70</sup>	1000+	...	Cusped, diamond-shaped	...
Inorganic (hard) templating	Carbon templating	...	0.5–400	Unimodal	Varies; often random	10
Polymer (soft) templating	Two-photon lithography	Au <sup>37</sup>	150	Architected by user	50	
	Polymer directed self-assembly	Ni <sup>2,38,39,42,43,47–49,68</sup>	20–40	Dependent on copolymer system; typically homogeneous in size and shape	5+	
		Au <sup>7</sup>	20		0.2	
	Polymer melt mixing	Pt <sup>55</sup>	40	Positively skewed relative to mean	Non-uniform	0.5
...		44	1000+		3000	
Polymer foaming	...	45	10,000+	Hierarchical	Round pores, random orientation	2000

to detail the fabrication of elemental metallic nanofoams.

A common method for the creation of nanoporous metals is dealloying. An active metallic species is selectively leached (chemically or electrochemically) from a binary alloy.<sup>13,14</sup> Dealloying produces pores of nanoscale dimensions in an assortment of metals with varying complexity in the pore size distribution. Alloys that have complete solubility across all compositions often yield nanoporous metals with unimodal pore size distributions. For example, nanoporous Au with fairly uniform pore sizes (5–200 nm) has been produced via dealloying of the globally miscible Au–Ag solid solution.<sup>3,5,15</sup> The presence of intermetallic compounds in alloy systems often produces nonunimodal pore size distributions upon dealloying. For example, dealloying of Au–Al alloys containing an Al<sub>2</sub>Au phase and a pure Al phase removes Al from both phases, leading to a bimodal nanopore size distribution.<sup>16</sup> As the number of intermetallic phases increases, so does the potential for complexity in the pore morphology of the resultant porous metal. Dealloying of rapidly solidified Al<sub>70</sub>Pd<sub>30</sub> comprised of Al<sub>3</sub>Pd and Al<sub>3</sub>Pd<sub>2</sub> phases has led to

a tortuous nanoporous Pd structure (3–25 nm) in the regions of native Al<sub>3</sub>Pd, while the native Al<sub>3</sub>Pd<sub>2</sub> regions demonstrated immunity to dealloying and remained intact, yielding a “composite” of nanoporous and solid metal regions.<sup>17</sup> With the adjustment of electrochemical parameters in dealloying processes and introduction of subsequent annealing, pore sizes can be tuned.<sup>3,5,15,17,18</sup> Dealloying for the creation of nanoporous metals is largely limited in scope to favor precious noble metals. However, Rahman et al. recently demonstrated the applicability of an analogous electrochemical dealloying technique to the Ni–Al system (Ni<sub>30</sub>Al<sub>70</sub>) to produce nanoporous nickel; the distribution of pore sizes was wider than that of traditional Au–Ag systems, and the process was highly sensitive to the composition of the parent alloy.<sup>19</sup> Similarly, nanoporous Cu has been synthesized via dealloying from a Cu–Al alloy.<sup>20</sup> In recent years, dealloying using a liquid metal instead of an aqueous solution has been developed to produce nanocomposites as well as nanoporous metals.<sup>21</sup> For example, an Nb–Ni alloy was immersed in molten Mg where Ni atoms were dealloyed (i.e., dissolved in Mg), and removal of the Mg–Ni phase by immersing the

composite in nitric acid leads to a porous Nb structure.<sup>22</sup> Porous Ti,<sup>23</sup> Fe, and Fe–Cr<sup>24</sup> have also been produced by a similar method.

Metallic foams have also been synthesized via controlled combustion of transition-metal complexes containing energetic ligands.<sup>4,6</sup> Porous iron monoliths exceeding an inch in length with extremely high surface area density have been prepared by the combustion reaction method. The mean pore size and pore size distribution can be tuned by modulating the ambient pressure during combustion; for example, combustion at 2.07 MPa leads to the coexistence of large pores in the 1–3  $\mu\text{m}$  regime and small pores in 20–200 nm range, while increasing the pressure to 7.33 MPa results in predominantly 20–200 nm pores.<sup>4</sup> Porous Co, Cu, and Ag with similar pore morphology have also been produced using this method.<sup>6</sup> In addition, electrodeposition of copper in a  $\text{CuSO}_4\text{--H}_2\text{SO}_4$  solution with nonsuppressed hydrogen evolution was demonstrated to facilitate porous metal formation with dendritic ligands; the resultant pores were predominantly 25–50  $\mu\text{m}$  in size, and the walls consist of loosely assembled short struts with sizes as small as 50 nm.<sup>25,26</sup>

Thermomechanical processing has also proven successful in the fabrication of porous metals and is widely applicable.<sup>27,28</sup> The simplest variety involves sintering of metal powders at elevated temperatures.<sup>27</sup> However, this method typically yields micrometer size pores that are largely a function of powder refining capability. Typical micron-scale spherical powders were shown to generate cusped pore shapes.<sup>27</sup> In the case of aluminum, uniaxial pressing during sintering accelerated the densification process and adjusted the final structure porosity (5–35%).<sup>27</sup> In some cases, space-holder particles are used during sintering which can later be selectively removed through melting (e.g., PMMA polymer<sup>29</sup>), dissolution (e.g., saccharose<sup>29</sup>), or evaporation processes (e.g., NaCl salt crystals,<sup>28</sup> Mg powder in Al<sup>27</sup>). This approach is widely used in various elemental metal and alloy systems to improve controllability of the final pore structure and the size distribution.<sup>30</sup>

The pore size  $d$  and sample dimension  $D$  of nanoporous metals from various fabrication methods reported in representative works are compiled in Fig. 1. NPMs from dealloying mostly have average  $d$  ranging from 3 nm to about 1  $\mu\text{m}$  and  $D$  between 1  $\mu\text{m}$  and 1 mm. Aside from dealloying, the aforementioned experimental procedures have mostly proven successful only in the synthesis of mesoporous metals with a wide pore size distribution involving large pore sizes (e.g., above 0.4  $\mu\text{m}$ ) (but with millimeter to centimeter sized samples), underlining the inherent challenge of assembly and stability in the fabrication of nanoporous metals with homogeneously-sized nanopores. Contrastingly, uniform nanoscale porosity in metals can be reliably achieved

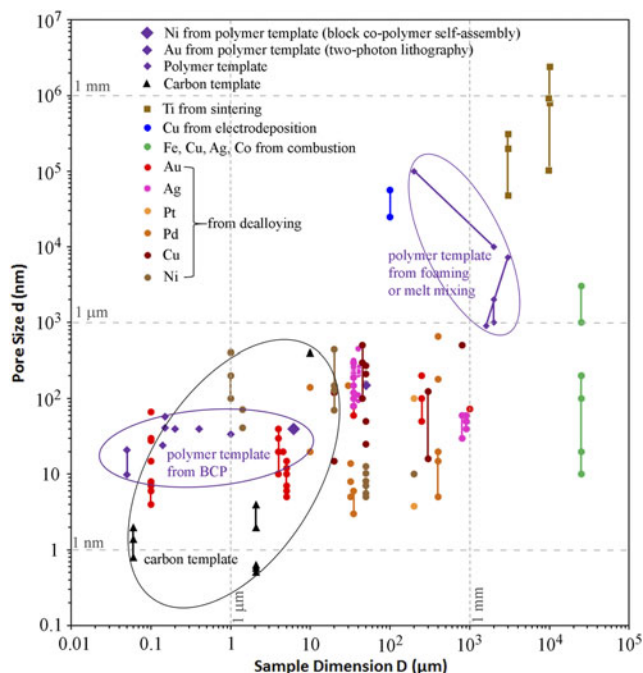


FIG. 1. Sample dimensions and pore sizes of nanoporous metals (or templates) fabricated by various methods, including Ni from polymer templates prepared by BCP self-assembly,<sup>2,68</sup> Au lattice from polymer templates prepared by two-photon lithography,<sup>37</sup> Ti from powder sintering,<sup>69,70</sup> Cu from electrodeposition,<sup>25,26</sup> Fe, Cu, Ag, Co from combustion,<sup>4</sup> Au,<sup>3,15,16,71–80</sup> Ag,<sup>18,80–84</sup> Pt,<sup>80,85</sup> Pd,<sup>17,80,86–89</sup> Cu,<sup>20,90–94</sup> and Ni<sup>19,95–98</sup> from dealloying, as well as carbon template,<sup>4</sup> and polymer templates fabricated by foaming,<sup>45</sup> melt mixing,<sup>44</sup> and BCP self-assembly.<sup>38,42,47–49,68</sup> Lines in the figure represent a range of pore sizes or sample sizes.

using templating methods involving deposition of metals onto a porous, sacrificial template that is subsequently removed. As shown in Fig. 1, porous templates can achieve uniform pore sizes as small as sub-nanometer to a few dozens of nanometers.

The main goal of this article is to provide a review of contemporary templating methods used to fabricate nanoporous metals with uniform pore sizes, with a particular focus on polymer template-based methods. A general description of templating methods will be provided in Sec. II. In Sec. III, we will discuss the fabrication of nanoporous polymeric templates, which have empirically demonstrated functionality in nanoporous metal fabrication. Deposition of metals onto polymer templates will be discussed in Sec. IV and removal of templates in Sec. V. Critical fabrication process discoveries and limitations will be noted.

## II. TEMPLATE-BASED FABRICATION OF NANOPOROUS METALS

Templates act as a support scaffold for metallization procedures in the fabrication of porous metals, enabling a robust processing approach which addresses fundamental difficulties in nanoporous metal assembly and

stability. By utilizing the nanoscale architectures more readily present in other material systems, metals in nontraditional nanoporous forms can be synthesized with a high degree of pore uniformity and organization. Template-based nanoporous metal fabrication methods generally involve three processing steps (template synthesis, metallization of template, and template removal), outlined in the process flow chart in Fig. 2. As the nanostructural form of the final nanoporous metal is largely determined by the pore dimensions and morphology of the template, template synthesis plays a pivotal role in the process. Physical vapor deposition and electrochemical/chemical plating techniques are potential methods for template metallization. There are two essential processing requirements for metallization. First, the process must yield sufficient metallic penetration into the template pores so as to create a continuous metallic network. Metallization also requires that the deposited metal be structurally supportive of its own mass for stability after eventual template removal; this requirement is related to template geometry. Sacrificial removal of the template ultimately yields a porous metal with a newfound structure representing the negative of the template. Template removal procedures vary between template species.

### A. Hard templates

Templating processes for material assembly are traditionally classified according to the properties of the template. Hard templating methods make use of inorganic templates such as porous carbon materials. Carbide-derived carbon materials can contain uniform nanopores with sizes as small as 0.65–2.1 nm, and Fig. 3(a) shows one such material derived from  $\text{Ti}_3\text{SiC}_2$  (chlorination in pure chlorine leads to Ti and Si extraction and carbon formation).<sup>31</sup> Porous carbon has also been prepared by the templating method [see Figs. 3(b)–3(d)], i.e., by infiltrating the pores (e.g., with sizes ranging from 2.5<sup>32</sup>–220 nm<sup>33</sup>) of the template with a carbon precursor followed by carbonization and template removal. For example, carbonization of zeolite Y is reported to have a periodicity of 1.4 nm, while porous carbon prepared via mesoporous silica can be produced with high-aspect-ratio pores of 400 nm diameter and up to 10  $\mu\text{m}$  in depth

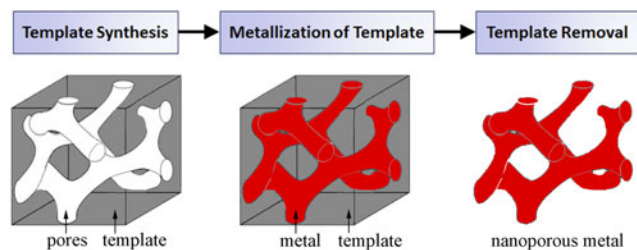


FIG. 2. A general process flow for template-based synthesis of nanoporous metals.

[Fig. 3(b)].<sup>33</sup> These templates have notable merit in their depth of porosity, extending beyond the micrometer scale, and their ease of template removal via burning after metallization. Electrodeposition of metals (such as Au, Cu, Ni,<sup>34</sup> and Fe<sup>35</sup>) into porous silicon was also demonstrated, but template removal was not attempted.

### B. Soft templates

Soft templating processes make use of less rigid, polymeric templates.<sup>36</sup> For example, sacrificial nanoscale polymer architectures are printed for templating purposes utilizing two-photon lithography,<sup>37</sup> and metallic lattices are produced after sputtering of an oxidation-resistant metal (e.g., gold) onto the template and removal of the template. This method provides excellent controllability of metal morphology on the nanoscale (10 nm resolution) and can produce features with 150 nm feature size but is typically used to form truss structures instead of bicontinuous pore-ligand or gyroid structures.<sup>37</sup> On the other hand, the stability of nanoscale domains in selected species of polymers has been demonstrated, making template-based fabrication appealing in this regard. Polymeric template formation for nanoporous metal fabrication is most commonly conducted using the self-organizing behavior of block copolymers (BCPs). Alternatively, melt mixing or foaming methods can also be used. Metallization of polymer templates by various metals (typically demonstrated with nickel) can be conducted via deposition.<sup>1</sup> Template removal after metallization can be achieved by using polymeric solvents or by thermal degradation of sacrificial scaffolds. Providing a high

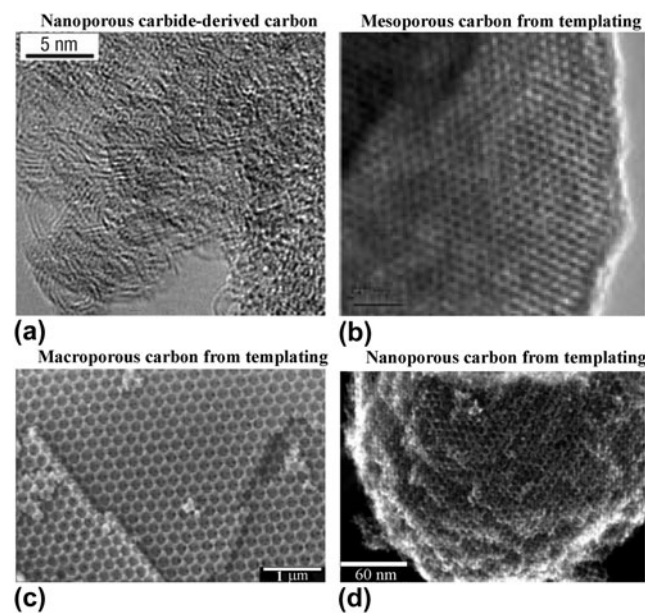


FIG. 3. Representative porous carbon templates (adapted from Refs. 31–33 with permissions). (a) Porous carbide-derived carbon,<sup>31</sup> (b–d) Porous carbon prepared using mesoporous silica templates,<sup>33</sup> inverse silica opal templates,<sup>33</sup> and MCM-48 silica templates,<sup>32</sup> respectively.

degree of structural uniformity and versatility in compatible metals, polymeric templating methods for the fabrication of nanoporous metals are positioned to reinvigorate contemporary efforts in this arena.

## 1. Using soft templates formed via block co-polymer self-assembly

BCP self-assembly can be exploited to form the sacrificial soft template structure.<sup>1,38,39</sup> BCPs are particularly apt to be used for templating purposes due to their tendency to microphase separate into spatially uniform, homogeneously sized nanoscale domains.<sup>40</sup> Use of well-known BCP systems allows for templates of varying morphologies (e. g., hexagonal-cylinder, double gyroid) to be easily produced based upon the thermodynamic understanding of the parent polymer system. Furthermore, domain size tuning is possible with the modulation of parent polymer block molecular weights and compositions.

Hashimoto et al. carried out a BCP self-assembly process using a polystyrene-*block*-polyisoprene (PS-*b*-PI) system, and a bicontinuous double gyroid nanostructure was naturally self-assembled.<sup>41</sup> Selective dissolution of the PI domains led to porous PS with bicontinuous and periodic nanochannels with diameter between 20 and 30 nm, and a typical area in the PS template is shown in Fig. 4(a). Subsequent nickel metallization of the soft PS templates via an electroless plating process was successfully demonstrated. However, the PS template removal was not conducted to obtain a standalone nanoporous nickel specimen. The premise of this research substantiated the feasibility of soft template-based fabrication of nanoporous metals. This method has since been adapted to a wide variety of polymer systems for the synthesis of templates.<sup>40</sup>

Following earlier studies which suggested that PS-*b*-PLLA polymers could be processed to adopt the double gyroid nanostructure (often referred to simply as “gyroid” structure),<sup>42,43</sup> Hsueh et al. analogously fabricated nanoporous nickel utilizing a double gyroid nanostructured template produced by the polystyrene-*block*-poly-L-lactide (PS-*b*-PLLA) system.<sup>2</sup> Pore sizes around 40 nm were obtained in the PS template [Fig. 4(b)] after selective removal of PLLA blocks, confirming the ability of PS-*b*-PLLA to phase separate with ligands on the nanoscale.<sup>2</sup> Nickel electrolessly plated onto the PS templates demonstrated stability after template removal, indicating that the bicontinuous nature of a double gyroid morphology provides sufficient metal connectivity for structural stability. The nanoporous nickel contained a desirable, uniform arrangement of homogeneously sized pores with approximately the same dimensions as that of the template.<sup>2</sup> Due to the ease of which PLLA can be selectively removed from PS-*b*-PLLA assemblies and the ability of this polymeric system to form the

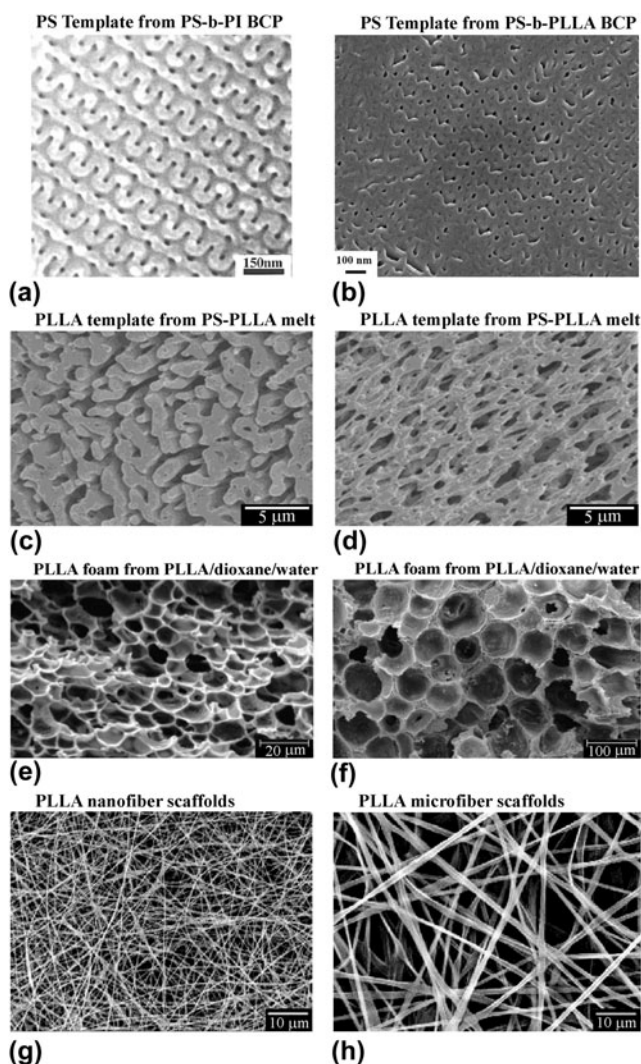


FIG. 4. Representative porous polymeric templates (adapted from Refs. 2, 41, and 44–46 with permissions). (a, b) Polystyrene (PS) templates from PS-*b*-PI<sup>41</sup> and PS-*b*-PLLA<sup>2</sup> BCP self-assembly. (c, d) Poly-L-lactide (PLLA) templates from PS/PLLA melt mixing.<sup>44</sup> (e, f) PLLA foams prepared by demixing from a PLLA/dioxane/water solution.<sup>45</sup> (g, h) PLLA fibrous scaffolds<sup>46</sup> made from nanofibers in (g) and microfibers in (h).

desirable double gyroid nanostructure, PS-*b*-PLLA BCPs are attractive for the formation of disposable templates. The PS-*b*-PLLA self-assembly method remains a cornerstone for the successful fabrication of nanoporous metals via templating.

## 2. Polymer templates formed via alternative methods

The versatile PS and PLLA polymer system can also be used to form porous template structures via methods other than directed BCP self-assembly. Due to the biocompatibility of PLLA and its readiness to form porous structures, research on this polymer species is proliferous.

Although not traditionally applied for template-based nanoporous metal fabrication purposes, research on the nanoscale assembly of PLLA affords realization of potential templating opportunities. Sarazin et al. demonstrated the ability for PS/PLLA blends to form porous template structures with sufficient structural integrity via melt mixing methods.<sup>44</sup> PS and PLLA polymer melts naturally segregate into ligand structures upon solidification, and the phase separation was found to be enhanced when a PS-*b*-PLLA compatibilizer was added to the mixture. In contrast to the aforementioned PS-*b*-PLLA self-assembly method, PS was removed via selective dissolution in cyclohexane leaving PLLA with a porous structure. The resultant PLLA pore size and continuity were strongly dependent on blend ratios. For example, Figs. 4(c) and 4(d) show a porous PLLA after PS extraction for blend ratios of PLLA/PS = 50/50 and 40/60, respectively; the pore morphology changed drastically while there is a minor increase in pore size as the volume fraction of PS increased from 50 to 60%. Most pore sizes exceeded 1  $\mu\text{m}$  and were generally between 1 and 4  $\mu\text{m}$ .<sup>44</sup> However, addition of more PS-*b*-PLLA compatibilizers demonstrated the ability to effectively reduce the mean pore size. Further pore size tuning via annealing was also conducted. This method generally lacks control over pore arrangement and the ability to produce nanoscale features. Metallization of these microporous templates was not attempted.

Another polymer melt approach involving demixing (phase separation) of a PLLA/dioxane/water solution was utilized to fabricate microporous PLLA foams.<sup>45</sup> Figure 4(e) shows a porous PLLA sample with a pore size of 10–15  $\mu\text{m}$  prepared by demixing at 25 °C for 5 min, while larger pore sizes of 40–90  $\mu\text{m}$  and porosity as high as 90% shown in Fig. 4(f) were obtained at 30 °C for 45 min. A high degree of pore interconnectedness was observed and was attributed to a spinodal decomposition process in addition to bimodal demixing.<sup>45</sup> This method demonstrates a reliable way to form mesoscale structures with hierarchical pore size distributions and highly interconnected pores that are compatible with the general templating concept.

Electrospinning of PLLA fibers is an additional method by which nanoscale assemblies could possibly be fabricated for templating. This technique can yield interconnected PLLA fibrous scaffolds, and control of fiber diameter was demonstrated for fibers down to 250 nm in diameter.<sup>46</sup> PLLA fibrous scaffolds made from nanofibers with diameters around 250 nm and from microfibers with diameters around 1.25  $\mu\text{m}$  are shown in Figs. 4(g) and 4(h), respectively. However, metallization of the PLLA scaffolds has not been demonstrated, and the feasibility of this technique for nanoporous metal fabrication is still unknown.

Although each of the outlined alternative template fabrication methods has demonstrated capability in forming polymers with microscale features, use of these methods for nanoporous metal synthesis has yet to be demonstrated. Furthermore, these methods generally do not provide sufficient pore homogeneity and spatial uniformity desirable in the fabrication of nanoporous metals. For this reason, template formation via BCP-directed self-assembly represents one of the most promising avenues for achieving spatially organized and homogeneously sized nanoscale pores. While many BCP systems are able to self-assemble into double gyroid structures, the PS-*b*-PLLA system has been demonstrated in the context of nanoporous metal fabrication.<sup>2</sup> Therefore, in the following section, we will primarily elaborate on the synthesis of nanoporous PS templates from PS-*b*-PLLA BCPs.

### III. SYNTHESIS OF NANOPOROUS POLYMERIC TEMPLATES FROM BCPs

Figure 5 presents a detailed flow chart for the synthesis of nanoporous polymer templates utilizing BCPs. After preparing the polymer solution and depositing the solution on a substrate, subsequent solvent evaporation and thermal annealing lead to BCPs with microphase separation. Porous polymeric templates are obtained by degrading sacrificial polymeric blocks. These processes are described in detail below. We will primarily discuss the fabrication of nanoporous PS templates using the PS-*b*-PLLA system, and some other BCP systems will be briefly discussed as well.

#### A. Preparing polymer solution

For PS-*b*-PLLA self-assembly, the gyroid morphology forms from low molecular weight BCP formulations at

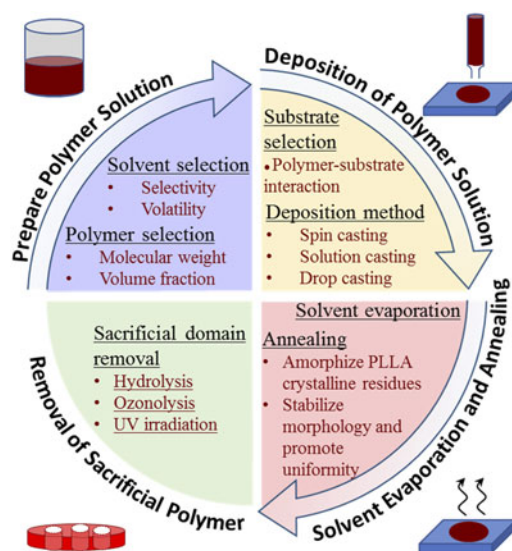


FIG. 5. Illustration of process flow for fabrication of nanoporous polymeric templates utilizing BCPs.

a PLLA volume fraction around 0.35.<sup>42</sup> At a similar volume fraction of 0.39, the PS-*b*-PLLA double gyroid morphology was produced using higher molecular weight polymer components (PS: 34 kg/mol, PLLA: 27 kg/mol).<sup>2</sup> Solvent annealing can also be used to facilitate the PS-*b*-PLLA assembly with improved lateral order.<sup>38,39</sup> Block co-polymer molecular weight and polymeric volume fractions were found to directly affect the resultant template pore size and uniformity in the case of the hexagonal cylinder pore morphology<sup>42,47</sup>; increasing the polymer block molecular weight yielded larger pores with improved homogeneity in pore size. Thus, the formulation or selection of the parent PS-*b*-PLLA polymer offers an opportunity for tuning the pore morphology and homogeneity in the resultant porous template.

As assembly of BCPs requires a high degree of chain mobility, liquidizing solvents facilitate the process of nanoscale domain separation between dissimilar copolymer species during evaporation processes. In turn, solvent choice, i.e., solvent selectivity and volatility, has a pronounced effect on the assembled morphology of BCPs.<sup>47</sup> In the case of solution casting, PS-selective solvents (such as chlorobenzene, tetrahydrofuran (THF), and benzene), which more readily dissolve PS than PLLA, were found to induce a favorable BCP nano-assembly whereas neutral solvents did not yield an appreciable polymeric organization.<sup>47</sup> It has been shown that PS-selective solvents with moderate volatilities (such as chlorobenzene with 12 mmHg vapor pressure) yielded more homogeneous nanoscale assemblies than those with high volatility.<sup>47</sup> It can be hypothesized that the pore size uniformity is correlated with the permissible time for assembly before complete evaporation. As self-assembly time is largely limited to the time it takes the solvent to evaporate, the slower evaporation rates of lower volatility solvents provide more time for polymer organization. This increase in polymer organizational homogeneity with decreasing solvent volatility may have a lower bound somewhere below a solvent vapor pressure of 12 mmHg.<sup>47</sup> In contrast to the PS-selective solvents prescribed for solution casting procedures, nonselective solvents demonstrated the ability to yield a template assembly when used in spin casting procedures.<sup>47</sup> Volatile dichloromethane is commonly used to facilitate gyroid nano-assembly in the PS-*b*-PLLA system via spin casting.<sup>2,47</sup>

## B. Deposition of polymer solution on substrate

To obtain nanoscale organization within the PS-*b*-PLLA polymer system, a solution deposition and solvent evaporation process is required. Several deposition methods have been documented, each yielding a distinct template morphology. Spin casting methods may be used for the preparation of thin-film templates, with thicknesses between 30 and 200 nm.<sup>47</sup> Adapting Lin et al.'s

work with the PS-*b*-PEO system,<sup>48</sup> spin casting of a dilute (1.5 wt%) PS-*b*-PLLA polymer solution onto a silicon wafer was shown to provide sufficient kinetic energy for copolymer self-organization into a hexagonal cylinder morphology with uniformity in arrangement and size.<sup>47,48</sup> The spin casting procedure affords flexibility in choice of the polymer solvent, whereas solution casting methods largely require the use of PS-selective solvents.<sup>47</sup> For the preparation of thicker microscale templates, solution casting has been used. Solution cast PS-*b*-PLLA at room temperature for a period of two weeks was shown to yield templates with a nanoscale double gyroid morphology and thickness on the order of centimeters.<sup>2</sup> Another possible method by which a polymer solution may be deposited on a substrate is drop casting, although it has not been widely applied to the PS-*b*-PLLA system. In the case of drop casting of the PS-P4VP polymeric system,<sup>49</sup> self-assembly into the nanostructured hexagonal cylinder morphology was mediated by hydrogen bonding between the P4VP block and added resorcinol.

Substrate selection may also affect the final template morphology for the PS-*b*-PLLA system. In the case of thin-film templates (thickness <100 nm), polymer-substrate interactions (such as polar interactions of PLLA with the hydrophilic surface when using a glass substrate<sup>47</sup>) are likely to have a slight effect on the morphology of the final polymer templates. This typically is manifested by the preferential wetting of glass or other polar substrates by the PLLA block, forming a base layer of PLLA below the assembled BCP morphology. Despite the presence of this PLLA base layer, it has been found that organizational homogeneity of the remaining template nanostructure was not greatly affected.<sup>47</sup> Similar morphology was reliably produced using a spin coating procedure for all the substrates tested, including glass slides, carbon-coated glass slides, indium tin oxide glass, silicon wafers, etc.<sup>47</sup>

## C. Solvent evaporation and annealing

Evaporation of the solvent, typically requiring days in open air environments, can promote microphase separation in the polymer film. For example, a PLLA hexagonal cylinder morphology was partly attributed to differences in permeation between the PS and PLLA blocks, and the efficiency of solvent evaporation is enhanced with microphase-separated microdomains.<sup>47</sup> Because this assembly process is mediated by evaporation at the film surface, there might be some limitations for assembled film thickness. Subsequent to the evaporation step, solid polymer thin films are sometimes further dried using a vacuum oven (e.g., in some cases they were desiccated for three days at 65 °C<sup>2,47</sup>).

A commonly used annealing procedure for dried, phase-separated BCPs aims to convert structurally-disturbing crystalline PLLA back to its amorphous state

to improve the microphase morphology. By heating to a temperature above the melting temperature of crystalline PLLA but below the Order–Disorder Transition (ODT) (i.e., 175 °C for 1–3 min), PLLA becomes amorphous within dried thin films; this acts to reduce the negative effect PLLA crystallinity has on the formation of the nanoscale morphology.<sup>2,42,47</sup> While not a required processing step, an additional thermal annealing treatment of templates at a temperature below the ODT temperature promotes uniformity in structure, long-range order, and thermodynamic stability of the polymer morphology.<sup>42,47,50,51</sup> It is critical that the ODT temperature is not exceeded during this heat treatment, or the polymer will reversibly transform back into a miscible melt. The ODT temperature for the PS-*b*-PLLA system ranges from ~180 to 280 °C as the total polymer molecular weight is increased,<sup>42</sup> and is around 230–240 °C at the optimal total polymer molecular weight (13.3–15.0 kg/mol) for the formation of a gyroid nanostructure. A three hour anneal at 140 °C followed by rapid quench to room temperature was reported to aid morphological stabilization of various thin-film PS-*b*-PLLA structures.<sup>42</sup> Alternatively, environmentally controlled solvent vapor annealing methods have demonstrated success in promoting morphological homogeneity and lengthening the span of the organization to nearly 10 μm for similar BCP systems (e.g., PS-*b*-PLA).<sup>50</sup>

### D. Selective removal of PLLA

To complete the process of fabricating sacrificial porous PS templates for metallization, PLLA nanodomains must be selectively removed from the assembly. It is common practice to hydrolyze PLLA with a solution of sodium hydroxide, such as a 0.5 M NaOH solution prepared with a 40/60 volumetric mixture of methanol and water.<sup>2</sup> Complete PLLA removal requires days to allow for sufficient percolation of the solution through the developing pores. The porous PS templates may be recovered from the hydrolyzing solution by using cell strainers. Gently washing the templates with dilute methanol is permissible.<sup>2</sup> For the PS-*b*-PI system, PI domains were selectively degraded by ozonolysis, i.e., by exposing the film to an atmosphere of ozone at room temperature for 24 h and subsequently soaking the film in ethanol.<sup>41</sup> PMMA was removed from PS-*b*-PMMA BCPs by the application of UV irradiation followed by rinsing.<sup>52</sup>

The process for fabricating porous PS templates from PS-*b*-PLLA polymer solutions is inherently time-consuming (it can take up to a month<sup>2</sup>) and is highly sensitive to processing parameters. Nonetheless, it provides a feasible pathway to the attainment of structurally homogeneous nanoporous templates. With the continued realization of improvements to the outlined process, this

method will continue gaining utility for the creation of nanoscale structures.

## IV. METALLIZATION OF NANOPOROUS POLYMERIC TEMPLATES

### A. Overview of metallization methods

The polymer template-based method for nanoporous metal fabrication involves a metallization procedure in which a metal must be deposited into tortuous nanopores. Physical vapor deposition is a viable option, although the line-of-sight method may encounter challenges in the infiltration of narrow or tortuous template pores.<sup>34</sup> Although promising, chemical vapor deposition processes have yet to be fully explored in the context of nanoporous metal fabrication.<sup>53</sup> Standard electroplating of complex geometries may yield poor uniformity of metallization because the localized current density varies across surfaces.<sup>34,54</sup> However, electrodeposition of Au and Pt into polymeric templates was successfully demonstrated.<sup>7,55</sup> Electrochemical deposition of Au into pore space of the PS-polyethylene oxide (PEO) template involved a nucleation step (1–3 cyclic voltammetry scans between 0 and –1.2 V at a rate of 50 mV/s) and a deposition step (at a fixed potential of –0.8 V for 100 s); the resulting nanoporous Au structure is promising as a 3D optical metamaterial with reduced plasma frequency compared to solid Au.<sup>7</sup> Electrodeposition of Pt into poly(4-fluorostyrene) (PFS) templates was carried out in one step with the working electrode at 0.1 V in a standard 3-electrode cell using a C<sub>16</sub>H<sub>2</sub>Pt solution.<sup>55</sup>

Electroless metal plating is a common method by which template metallization is achieved in the literature.<sup>56</sup> It involves auto-catalyzed electrochemical reactions in an ionic solution that enables enhanced infiltration of narrow pores.<sup>34,35,56</sup> Electroless plating is attractively generalizable to a wide range of metals: nickel,<sup>2,41,57</sup> copper,<sup>58</sup> gold,<sup>56</sup> silver,<sup>56</sup> cobalt,<sup>57</sup> and iron.<sup>59</sup> In particular, extensive research has been conducted for the electroless plating of nickel onto various polymer substrates.<sup>60</sup> Excellent uniformity in thickness of the deposited nickel and coverage of complex geometries can be obtained.<sup>54</sup>

### B. Electroless plating

Hashimoto et al.<sup>41</sup> and Hsueh et al.<sup>2</sup> have reported successful electroless plating of nickel onto porous polystyrene (PS) with pore sizes below 50 nm. Figures 6(a) and 6(b) show Transmission Electron Microscopy (TEM) images of PS–Ni gyroid nanohybrids reported in Refs. 41 and 2, respectively. In both cases, the prior pore space in PS was replaced with Ni. Electroless Ni plating was also applied to nanoporous PS templates where PS struts were covered with a layer of poly(4-vinylpyridine) (P4VP), which is hydrophilic and facilitates the penetration of

water-based plating reagents into the pore channel.<sup>61</sup> A bright-field TEM image of the Ni-plated PS/P4VP template is shown in Fig. 6(c). Homogeneous distribution of Ni seen in Fig. 6(c) suggests that the prior pore space is well connected and is accessible for the plating solution. Ni was also successfully plated into nanochannels in a bicontinuous double gyroid template containing PS,<sup>62</sup> as shown in Fig. 6(d).

## 1. Electroless deposition process

Figure 7 presents the process flow for metallization of nanoporous polymeric templates by electroless deposition. Electroless plating of nickel onto polymer is generally performed in three steps: sensitization, activation, and plating.<sup>41</sup> The sensitization and activation steps prepare the polymeric template surfaces for metallization.

(i) Sensitization of nanoporous PS substrates is the primary enabler of the metallization process and can be performed in several ways. Traditionally, PS templates have been sensitized utilizing  $\text{SnCl}_2$  as a seeding agent for the activation step, i.e., the templates were soaked in an aqueous solution of  $\text{SnCl}_2$ . However, this depends on the ability of  $\text{Sn}^{2+}$  ions to adhere to the surface of the nanochannels in the template.<sup>41</sup> An alternative sensitization process employs a surface modification technique

that enhances the ability of metallizing ions to adhere to the pore surfaces. For example, through soaking PS templates in poly(allylamine hydrochloride) (PAH) for 30 min, PAH attachment to the surfaces reduces hydrophobicity and permits subsequent seeding during activation.<sup>60</sup> Similar surface modification approaches have been demonstrated for bulk ABS<sup>63</sup> and PP<sup>64</sup> and could be applicable to many more polymeric species.

(ii) Following sensitization, templates are immersed in a palladium solution (commonly  $\text{PdCl}_2$  or  $\text{Na}_2\text{PdCl}_4$ ) for activation. For the Sn-based sensitization method, this activation process is achieved via a redox reaction in which Pd is reduced on the surface of the template, and  $\text{Sn}^{2+}$  ions previously adsorbed on the nanochannel surfaces are converted to  $\text{Sn}^{4+}$ . It has been shown that the Sn sensitization step may not be necessary for the electroless plating of nickel onto porous PS templates<sup>2</sup>; in this case, the sensitization step is foregone and Pd ions directly adhere to the porous templates. However, it was shown in a different study that appreciable Pd attachment to a bulk PS surface is not possible without template sensitization due to the hydrophobic nature of polymer surfaces.<sup>60</sup> Following the PAH surface modification sensitization method, Pd ions are directly adhered to the PAH-modified pore surfaces in the PS template. The imbedded palladium seeds within the porous template structure act as nuclei for subsequent nickel plating.

(iii) Upon introducing activated templates to an ionic nickel plating bath, nickel ions are reduced at palladium sites where Pd acts as catalyst of the reduction of  $\text{Ni}^{2+}$  to Ni. In general, electroless plating processes are auto-catalyzed as redox reactions. Because nanoporous metal templates have high specific surface areas, plating often

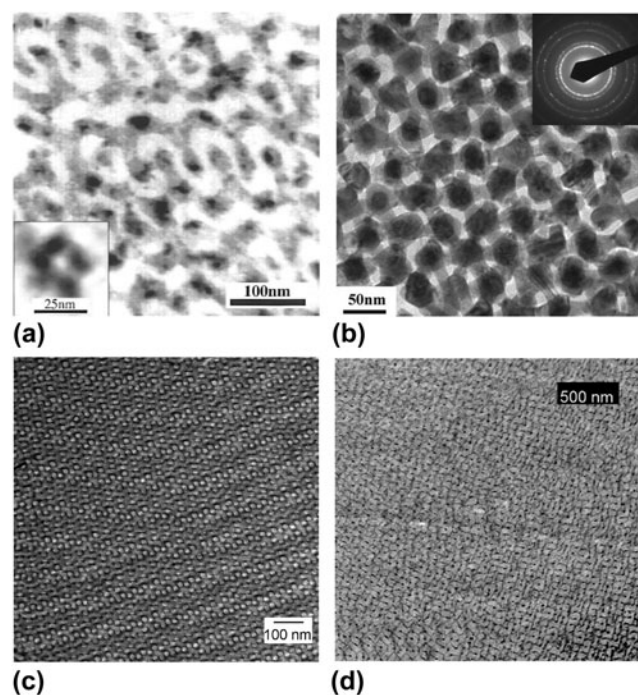


FIG. 6. TEM images of polymer-nickel gyroid nanohybrids without staining (Ni domains appear dark) reported in Refs. 2, 41, 61, and 62 (reproduced with permissions). These images were taken after electroless plating of Ni into nanochannels in the porous template but before removal of polymer template. The polymer templates are PS<sup>2,41</sup> in (a, b), PS/P4VP<sup>61</sup> in (c), and PrOS/PS/P4VP<sup>62</sup> in (d).

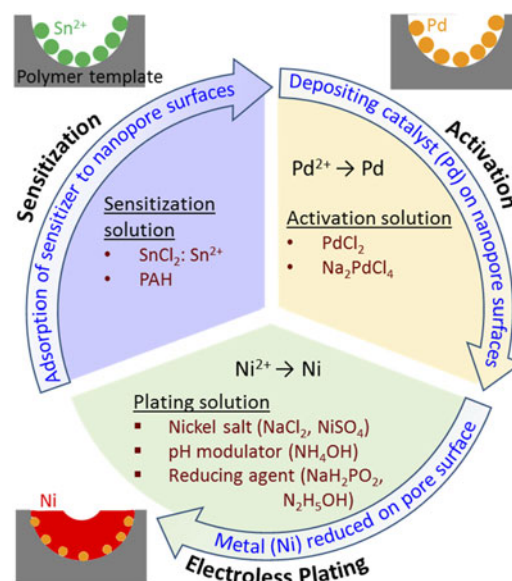


FIG. 7. Illustration of the process flow for metallization of nanoporous polymer templates by electroless plating of nickel.

requires refreshing of the Ni bath to avoid drastic Ni ion depletion in solution.<sup>65</sup>

## 2. Kinetics of electroless deposition

Properties of the plating bath, such as temperature, pH, and reducing agent content, have a strong effect on plating kinetics. Most electroless plating baths contain common functional components: an ionic metal in solution to be plated, a pH modulator, and a reducing agent. (i) In the case of electroless nickel plating, it is common to employ hydrated nickel salts (i.e.,  $\text{NiCl}_2 \cdot 6\text{H}_2\text{O}$ ,  $\text{NiSO}_4 \cdot 6\text{H}_2\text{O}$ ) for supplying nickel ions.<sup>2,66</sup> (ii) Bath pH is typically controlled via addition of liquid ammonia.<sup>2,66</sup> In general, basic solutions provide optimal plating kinetics for electroless nickel deposition.<sup>66,67</sup> (iii) Nickel plating can be driven through the addition of reducing agents, such as sodium hypophosphate, to the bath.<sup>54</sup> Sodium hypophosphite is commonly used to improve reduction kinetics of plating at the appropriate concentrations, but it is known to introduce phosphorous content to the plated nickel metal.<sup>66</sup> Hsueh et al. used hydrazinium hydroxide as an alternative reducing agent; they also added ethanol to their plating bath, likely to promote wetting of the nanopores for a successful deposit.<sup>2</sup>

Understanding the reaction kinetics of electroless Ni plating procedures is crucial for sufficient metallization of PS templates but is challenging due to the complexity of plating baths and the large number of variables that affect plating (e.g., substrate, pretreatment method, temperature, pH, reducing agent concentration). Variation in nickel adhesion to various substrates adds additional complexity. Plating kinetics for nickel onto PS is not well documented in the literature. However, general processing insights can be gleaned from experiments conducted for electroless Ni plating of alternative substrates. Zhang et al. found that surface treatment sensitizing procedures (such as those previously described) can affect an almost 3-fold increase in the Ni plating rate and improve deposit uniformity onto hollow glass spheres.<sup>66</sup> The optimal pH for Ni plating of glass spheres was reported to be 12.<sup>66</sup> An even more dramatic increase in the plating rate was evidenced for bulk PS substrates sensitized with PAH when compared to the baseline.<sup>60</sup> Normalizing to surface area, electroless Ni plating onto bulk PS has been demonstrated at a rate of approximately  $1.3 \mu\text{m}/\text{h}$ .<sup>60</sup> Guo et al. discovered a common trend in plating kinetics with temperature, pH, and reducing agent concentration for electroless Ni plating onto polyester fibers; as each parameter was increased, nickel deposition rates steadily increased before reaching a maximum [on the order of  $20 \text{ mg}/(\text{cm}^2 \text{ h})$ ] and then subsequently decreased.<sup>67</sup> The optimal plating conditions were found to be  $80^\circ\text{C}$ ,  $\text{pH} = 8.5$ , and  $[\text{NaH}_2\text{PO}_2] = 40 \text{ g/L}$ , respectively.<sup>67</sup>

Furthermore, an empirical kinetic equation taking the form of Eq. (1) was developed in this study and validated by experimental data.

$$v = a \cdot \exp\left[b \frac{(T - 333)}{T}\right] \left(\prod_i [X_i]^{n_i}\right), \quad (1)$$

where  $v$  is the deposition rate,  $T$  is the temperature, and  $[X_i]$  denotes the concentration of the  $i$ th ion.

## V. REMOVAL OF POLYMERIC TEMPLATES

Subsequent to metallization, the polymeric templates themselves must be sacrificially removed from the metallized assembly. There are several possible methods to remove the template.

(i) Polymer dissolution in volatile solvents, such as tetrahydrofuran (THF), are commonly used, and the process can take over twenty hours.<sup>2</sup> After sufficiently metallizing nanoporous gyroid PS templates by electroless deposition and selective dissolution of the PS scaffold, nanoporous Ni structures are obtained, [see Fig. 8(a)] and their structural stability has been demonstrated.<sup>2</sup>

(ii) Template removal may also be accomplished by decomposition of polymer at elevated temperatures (pyrolysis). For example, after electroless plating of Ni into the PS/P4VP template, the template was removed by

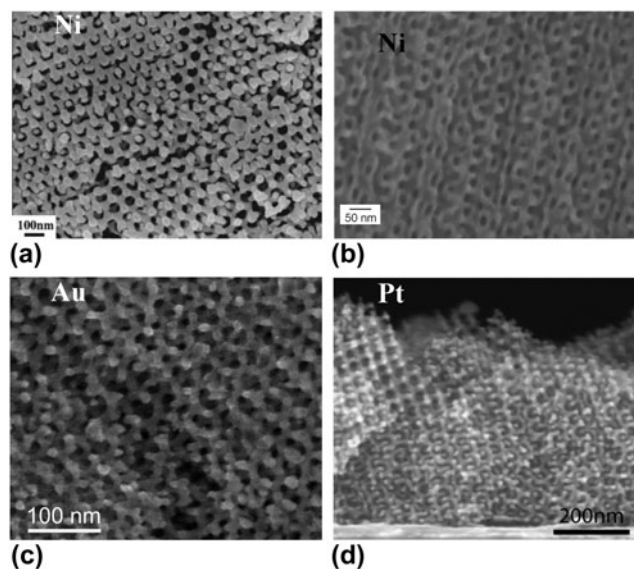


FIG. 8. SEM images of nanoporous metals after removal of polymeric templates (adapted from Refs. 2, 7, 55, and 61 with permissions). (a) Nanoporous Ni from electroless deposition of Ni into porous PS template followed by template dissolution.<sup>2</sup> (b) Nanoporous Ni from electroless deposition of Ni into PS/P4VP template and template removal by pyrolysis.<sup>61</sup> (c) Nanoporous Au from electrodeposition of Au into the PS/PEO template and template removal by plasma etching.<sup>7</sup> (d) Nanoporous Pt from electrodeposition of Pt into the PFS template and removal of the template by  $\text{O}_2$  plasma etching.<sup>55</sup>

heating at 350 °C while keeping the Ni structure intact as shown in Fig. 8(b).<sup>61</sup>

(iii) Plasma etching has also been utilized to remove polymer templates. Figure 8(c) shows nanoporous Au obtained from electrodeposition of Au into the PS/PEO template and template removal by plasma etching,<sup>7</sup> and Fig. 8(d) shows nanoporous Pt from electrodeposition of Pt into the PFS template and removal of PFS by O<sub>2</sub> plasma etching.<sup>55</sup> In both cases, template removal was considered successful, revealing stable nanoporous metallic structures.

The nanopore size is highly uniform in each nanoporous metal shown in Fig. 8, and the pore size is around 40 nm in Figs. 8(a) and 8(d) and 20 nm in Figs. 8(b) and 8(c).

## VI. CONCLUSIONS AND OUTLOOK

NPMs with novel properties, e.g., high surface area, high specific strength, and nontraditional functional behavior, are positioned to stimulate the applicability of metals in new high-performance applications. However, there are fundamental challenges in the fabrication of porous metallic materials with nanoscale pore sizes and interconnectivity. In this article, we present a critical review of nanoporous metal fabrication. We have briefly discussed traditional methods such as combustion and electrodeposition which typically do not produce nanoscale pores in metals, as well as the dealloying method, which has demonstrated success in producing nanoscale pores but typically leads to a wide pore size distribution and is mainly limited to noble metals. We have primarily focused on templating methods for nanoporous metal fabrication, which offer a wider range of applicable metals while enhancing control of the metallic pore morphology. Metals are introduced into the pore spaces of sacrificial nanoporous templates by deposition or infiltration, and subsequent removal of the templates yields nanoporous metals. While hard templating processes are also feasible, soft polymeric templates are most frequently used. The most common are nanoporous PS templates with the double gyroid structure obtained from the PS-*b*-PLLA block co-polymer system. Metallization of the porous polymer templates can be carried out by a variety of methods, although electroless plating has been the most commonly used method. Electroless plating permits uniform plating by many metallic species. Preparation of polymer templates and their subsequent metallization have been discussed at length.

The utility of the polymer template-based method for fabricating nanoporous metals has yet to be fully realized. The development of methods for increasing the assembly depth of BCP films and, therefore, the thickness of template samples to the micron-scale will further improve the applicability of porous metals in various applications.

Electroless plating of high surface area and nanostructured polymeric templates are not well understood; future work is required for providing a quantitative understanding of this process through study of pore penetration and template attachment by different metallic species. Development of porous template-compatible physical or chemical vapor deposition methods could also provide attractive alternative methods by which templates can be metalized. Additionally, mechanical and functional characterization of nanoporous metals is also an important area for investigation.

## ACKNOWLEDGMENTS

This work was primarily supported by the RPI start-up fund. T. Rebbecchi was also partially supported by the U.S. National Science Foundation grant DMR #1352524.

## REFERENCES

1. I. Vukovic, G. ten Brinke, and K. Loos: Block copolymer template-directed synthesis of well-ordered metallic nanostructures. *Polymer* **54**, 2591 (2013).
2. H.Y. Hsueh, Y.C. Huang, R.M. Ho, C.H. Lai, T. Makida, and H. Hasegawa: Nanoporous gyroid nickel from block copolymer templates via electroless plating. *Adv. Mater.* **23**, 3041 (2011).
3. E. Seker, M. Reed, and M. Begley: Nanoporous gold: Fabrication, characterization, and applications. *Materials* **2**, 2188 (2009).
4. B. Tappan, M. Huynh, M. Hiskey, D. Chavez, E. Luther, J. Mang, and S. Son: Ultralow-density nanostructured metal foams: Combustion synthesis, morphology, and composition. *J. Am. Chem. Soc.* **128**, 6589 (2006).
5. H-J. Qiu, L. Peng, X. Li, H. Xu, and Y. Wang: Using corrosion to fabricate various nanoporous metal structures. *Corros. Sci.* **92**, 16 (2015).
6. B.C. Tappan, S.A. Steiner, and E.P. Luther: Nanoporous metal foams. *Angew. Chem., Int. Ed.* **49**, 4544 (2010).
7. S. Vignolini, N.A. Yufa, P.S. Cunha, S. Guldin, I. Rushkin, M. Stefik, K. Hur, U. Wiesner, J.J. Baumberg, and U. Steiner: A 3D optical metamaterial made by self-assembly. *Adv. Mater.* **24**, OP23 (2012).
8. T. Kou, D. Li, C. Zhang, Z. Zhang, and H. Yang: Unsupported nanoporous Ag catalysts towards CO oxidation. *J. Mol. Catal. A: Chem.* **382**, 55 (2014).
9. A. Wittstock, V. Zielasek, J. Biener, C. Friend, and M. Bäumer: Nanoporous gold catalysts for selective gas-phase oxidative coupling of methanol at low temperature. *Science* **327**, 319 (2010).
10. C. Liu, E.I. Gillette, X. Chen, A.J. Pearce, A.C. Kozen, M.A. Schroeder, K.E. Gregorczyk, S.B. Lee, and G.W. Rubloff: An all-in-one nanopore battery array. *Nat. Nanotechnol.* **9**, 1031 (2014).
11. R.E. Morris and P.S. Wheatley: Gas storage in nanoporous materials. *Angew. Chem., Int. Ed.* **47**, 4966 (2008).
12. J. Zhang and C.M. Li: Nanoporous metals: Fabrication strategies and advanced electrochemical applications in catalysis, sensing and energy systems. *Chem. Soc. Rev.* **41**, 7016 (2012).
13. J. Erlebacher, M.J. Aziz, A. Karma, N. Dimitrov, and K. Sieradzki: Evolution of nanoporosity in dealloying. *Nature* **410**, 450 (2001).
14. J. Erlebacher and K. Sieradzki: Pattern formation during dealloying. *Scr. Mater.* **49**, 991 (2003).
15. Y. Liu, S. Bliznakov, and N. Dimitrov: Comprehensive study of the application of a pb underpotential deposition-assisted method

- for surface area measurement of metallic nanoporous materials. *J. Phys. Chem. C* **113**, 12362 (2009).
16. Z. Zhang, Y. Wang, Z. Qi, J. Lin, and X. Bian: Nanoporous gold ribbons with bimodal channel size distributions by chemical dealloying of Al–Au alloys. *J. Phys. Chem. C* **113**, 1308 (2009).
  17. X. Wang, W. Wang, Z. Qi, C. Zhao, H. Ji, and Z. Zhang: Fabrication, microstructure and electrocatalytic property of novel nanoporous palladium composites. *J. Alloys Compd.* **508**, 463 (2010).
  18. E. Detsi, M.S. Selles, P.R. Onck, and J.T.M. De Hosson: Nanoporous silver as electrochemical actuator. *Scr. Mater.* **69**, 195 (2013).
  19. M.A. Rahman, X. Zhu, and C. Wen: Fabrication of nanoporous Ni by chemical dealloying Al from Ni–Al alloys for lithium-ion batteries. *Int. J. Electrochem. Sci.* **10**, 3767 (2015).
  20. Y. Xing, S. Wang, B. Fang, S. Zhang, and W. Liu: Structure evolution of nanoporous copper by dealloying of Al 17–33 at.% Cu alloy. *Int. J. Electrochem. Sci.* **10**, 4849 (2015).
  21. P.-A. Geslin, I. McCue, B. Gaskey, J. Erlebacher, and A. Karma: Topology-generating interfacial pattern formation during liquid metal dealloying. *Nat. Commun.* **6**, 8887 (2015).
  22. J.W. Kim, M. Tsuda, T. Wada, K. Yubuta, S.G. Kim, and H. Kato: Optimizing niobium dealloying with metallic melt to fabricate porous structure for electrolytic capacitors. *Acta Mater.* **84**, 497 (2015).
  23. Y.-c.K. Chen-Wiegart, T. Wada, N. Butakov, X. Xiao, F. De Carlo, H. Kato, J. Wang, D.C. Dunand, and E. Maire: 3D morphological evolution of porous titanium by X-ray micro- and nano-tomography. *J. Mater. Res.* **28**, 2444 (2013).
  24. T. Wada and H. Kato: Three-dimensional open-cell macroporous iron, chromium and ferritic stainless steel. *Scr. Mater.* **68**, 723 (2013).
  25. H.-C. Shin and M. Liu: Copper foam structures with highly porous nanostructured walls. *Chem. Mater.* **16**, 5460 (2004).
  26. H.C. Shin, J. Dong, and M. Liu: Nanoporous structures prepared by an electrochemical deposition process. *Adv. Mater.* **15**, 1610 (2003).
  27. D.C. Dunand: Processing of titanium foams. *Adv. Eng. Mater.* **6**, 369 (2004).
  28. J.A. Scott and D.C. Dunand: Metallic sandwiches with open porosity facings and closed porosity cores for SOFC interconnects. *Mater. Sci. Eng., A* **585**, 32 (2013).
  29. M. Köhl, T. Habijan, M. Bram, H.P. Buchkremer, D. Stöver, and M. Köller: Powder metallurgical near-net-shape fabrication of porous NiTi shape memory alloys for use as long-term implants by the combination of the metal injection molding process with the space-holder technique. *Adv. Eng. Mater.* **11**, 959 (2009).
  30. W. Niu, C. Bai, G. Qiu, and Q. Wang: Processing and properties of porous titanium using space holder technique. *Mater. Sci. Eng., A* **506**, 148 (2009).
  31. Y. Gogotsi, A. Nikitin, H. Ye, W. Zhou, J.E. Fischer, B. Yi, H.C. Foley, and M.W. Barsoum: Nanoporous carbide-derived carbon with tunable pore size. *Nat. Mater.* **2**, 591 (2003).
  32. C. Liang, Z. Li, and S. Dai: Mesoporous carbon materials: Synthesis and modification. *Angew. Chem., Int. Ed.* **47**, 3696 (2008).
  33. X. Zhao, F. Su, Q. Yan, W. Guo, X.Y. Bao, L. Lv, and Z. Zhou: Templating methods for preparation of porous structures. *J. Mater. Chem.* **16**, 637 (2006).
  34. M. Jeske, J.W. Schultze, M. Thönissen, and H. Münder: Electrodeposition of metals into porous silicon. *Thin Solid Films* **255**, 63 (1995).
  35. F. Ronkel, J.W. Schultze, and R. Arens-Fischer: Electrical contact to porous silicon by electrodeposition of iron. *Thin Solid Films* **276**, 40 (1996).
  36. C. Rodríguez-Abreu, N. Vilanova, C. Solans, M. Ujihara, T. Imae, A. López-Quintela, and S. Motojima: A combination of hard and soft templating for the fabrication of silica hollow microcoils with nanostructured walls. *Nanoscale Res. Lett.* **6**, 1 (2011).
  37. L.C. Montemayor, L.R. Meza, and J.R. Greer: Design and fabrication of hollow rigid nanolattices via two-photon lithography. *Adv. Eng. Mater.* **16**, 184 (2014).
  38. M.-S. She, T.-Y. Lo, and R.-M. Ho: Controlled ordering of block copolymer gyroid thin films by solvent annealing. *Macromolecules* **47**, 175 (2014).
  39. M.-S. She, T.-Y. Lo, H.-Y. Hsueh, and R.-M. Ho: Nanostructured thin films of degradable block copolymers and their applications. *NPG Asia Mater.* **5**, e42 (2013).
  40. S.B. Darling: Directing the self-assembly of block copolymers. *Prog. Polym. Sci.* **32**, 1152 (2007).
  41. T. Hashimoto, K. Tsutsumi, and Y. Funaki: Nanoprocessing based on bicontinuous microdomains of block copolymers: Nanochannels coated with metals. *Langmuir* **13**, 6869 (1997).
  42. R.-M. Ho, Y.-W. Chiang, C.-K. Chen, H.-W. Wang, H. Hasegawa, S. Akasaka, E.L. Thomas, C. Burger, and B.S. Hsiao: Block copolymers with a twist. *J. Am. Chem. Soc.* **131**, 18533 (2009).
  43. R.-M. Ho, Y.-W. Chiang, C.-C. Tsai, C.-C. Lin, B.-T. Ko, and B.-H. Huang: Three-dimensionally packed nanohelical phase in chiral block copolymers. *J. Am. Chem. Soc.* **126**, 2704 (2004).
  44. P. Sarazin and B.D. Favis: Morphology control in Co-continuous poly(l-lactide)/polystyrene blends: A route towards highly structured and interconnected porosity in poly(l-lactide) materials. *Biomacromolecules* **4**, 1669 (2003).
  45. F.C. Pavia, V. La Carrubba, S. Piccarolo, and V. Brucato: Polymeric scaffolds prepared via thermally induced phase separation: Tuning of structure and morphology. *J. Biomed. Mater. Res., Part A* **86**, 459 (2008).
  46. F. Yang, R. Murugan, S. Wang, and S. Ramakrishna: Electrospinning of nano/micro scale poly(L-lactic acid) aligned fibers and their potential in neural tissue engineering. *Biomaterials* **26**, 2603 (2005).
  47. R.-M. Ho, W.-H. Tseng, H.-W. Fan, Y.-W. Chiang, C.-C. Lin, B.-T. Ko, and B.-H. Huang: Solvent-induced microdomain orientation in polystyrene-*b*-poly(L-lactide) diblock copolymer thin films for nanopatterning. *Polymer* **46**, 9362 (2005).
  48. Z. Lin, D.H. Kim, X. Wu, L. Boosahda, D. Stone, L. LaRose, and T.P. Russell: A rapid route to arrays of nanostructures in thin films. *Adv. Mater.* **14**, 1373 (2002).
  49. C. Liang, K. Hong, G.A. Guiochon, J.W. Mays, and S. Dai: Synthesis of a large-scale highly ordered porous carbon film by self-assembly of block copolymers. *Angew. Chem., Int. Ed.* **43**, 5785 (2004).
  50. A. Baruth, M. Seo, C.H. Lin, K. Walster, A. Shankar, M.A. Hillmyer, and C. Leighton: Optimization of long-range order in solvent vapor annealed poly(styrene)-block-poly(lactide) thin films for nanolithography. *ACS Appl. Mater. Interfaces* **6**, 13770 (2014).
  51. S.H. Kim, M.J. Misner, T. Xu, M. Kimura, and T.P. Russell: Highly oriented and ordered arrays from block copolymers via solvent evaporation. *Adv. Mater.* **16**, 226 (2004).
  52. T. Thurn-Albrecht, R. Steiner, J. DeRouchey, C.M. Stafford, E. Huang, M. Bal, M. Tuominen, C.J. Hawker, and T.P. Russell: Nanoscopic templates from oriented block copolymer films. *Adv. Mater.* **12**, 787 (2000).
  53. P. Delhaes: Chemical vapor deposition and infiltration processes of carbon materials. *Carbon* **40**, 641 (2002).
  54. R. Parkinson: *Properties and Applications of Electroless Nickel*, Vol. **37** (Nickel Development Institute, Toronto, Canada, 1997).
  55. E.J. Crossland, S. Ludwigs, M.A. Hillmyer, and U. Steiner: Control of gyroid forming block copolymer templates: Effects of an electric field and surface topography. *Soft Matter* **6**, 670 (2010).

56. N. Takeyasu, T. Tanaka, and S. Kawata: Metal deposition deep into microstructure by electroless plating. *Jpn. J. Appl. Phys.* **44**, L1134 (2005).
57. A. Brenner and G.E. Riddell: Deposition of nickel and cobalt by chemical reduction. *J. Res. Natl. Bur. Stand.* **39**, 385 (1947).
58. M. Paunovic: Electroless deposition of copper. *Mod. Electroplat.* **1**, 433 (2010).
59. M.A. Dinderman, W.J. Dressick, C.N. Kostelansky, R.R. Price, S.B. Qadri, and P.E. Schoen: Electroless plating of iron onto cellulose fibers. *Chem. Mater.* **18**, 4361 (2006).
60. W. Wang, S. Ji, and I. Lee: A facile method of nickel electroless deposition on various neutral hydrophobic polymer surfaces. *Appl. Surf. Sci.* **283**, 309 (2013).
61. I. Vukovic, S. Punzhin, Z. Vukovic, P. Onck, J.T.M. De Hosson, G. ten Brinke, and K. Loos: Supramolecular route to well-ordered metal nanofoams. *ACS Nano* **5**, 6339 (2011).
62. G.G. du Sart, I. Vukovic, Z. Vukovic, E. Polushkin, P. Hiekkataipale, J. Ruokolainen, K. Loos, and G. ten Brinke: Nanoporous network channels from self-assembled triblock copolymer supramolecules. *Macromol. Rapid Commun.* **32**, 366 (2011).
63. A. Garcia, T. Berthelot, P. Viel, A. Mesnage, P. Jégou, F. Nekelson, S. Roussel, and S. Palacin: ABS polymer electroless plating through a one-step poly(acrylic acid) covalent grafting. *ACS Appl. Mater. Interfaces* **2**, 1177 (2010).
64. S. Tengsuwan and M. Ohshima: Electroless nickel plating on polypropylene via hydrophilic modification and supercritical carbon dioxide Pd-complex infusion. *J. Supercrit. Fluids* **69**, 117 (2012).
65. M.J. Aleksinas: Troubleshooting Electroless Nickel Plating Solutions. In *Electroless Plating: Fundamentals & Applications*, G.O. Mallory and J.B. Hajdu, eds. (American Electroplaters and Surface Finishers Society, Orlando, Florida, 1990), pp. 101–110.
66. Q. Zhang, M. Wu, and W. Zhao: Electroless nickel plating on hollow glass microspheres. *Surf. Coat. Technol.* **192**, 213 (2005).
67. R. Guo, S. Jiang, C. Yuen, M. Ng, J. Lan, and G. Zheng: Influence of deposition parameters and kinetics of electroless Ni–P plating on polyester fiber. *Fibers Polym.* **13**, 1037 (2012).
68. H-Y. Hsueh, H-Y. Chen, M-S. She, C-K. Chen, R-M. Ho, S. Gwo, H. Hasegawa, and E.L. Thomas: Inorganic gyroid with exceptionally low refractive index from block copolymer templating. *Nano Lett.* **10**, 4994 (2010).
69. M. Bram, C. Stiller, H.P. Buchkremer, D. Stöver, and H. Baur: High-porosity titanium, stainless steel, and superalloy parts. *Adv. Eng. Mater.* **2**, 196 (2000).
70. M. Thieme, K-P. Wieters, F. Bergner, D. Scharnweber, H. Worch, J. Ndop, T. Kim, and W. Grill: Titanium powder sintering for preparation of a porous functionally graded material destined for orthopaedic implants. *J. Mater. Sci.: Mater. Med.* **12**, 225 (2001).
71. C. Ji and P.C. Seanson: Fabrication of nanoporous gold nanowires. *Appl. Phys. Lett.* **81**, 4437 (2002).
72. L. Liu, W. Lee, Z. Huang, R. Scholz, and U. Gösele: Fabrication and characterization of a flow-through nanoporous gold nanowire/AAO composite membrane. *Nanotechnology* **19**, 335604 (2008).
73. Y. Ding, Y.J. Kim, and J. Erlebacher: Nanoporous gold leaf: “Ancient technology”/advanced material. *Adv. Mater.* **16**, 1897 (2004).
74. A. Dursun, D. Pugh, and S. Corcoran: Dealloying of Ag–Au alloys in halide-containing electrolytes affect on critical potential and pore size. *J. Electrochem. Soc.* **150**, B355 (2003).
75. T. Fujita, P. Guan, K. McKenna, X. Lang, A. Hirata, L. Zhang, T. Tokunaga, S. Arai, Y. Yamamoto, N. Tanaka, Y. Ishikawa, N. Asao, Y. Yamamoto, J. Erlebacher, and M. Chen: Atomic origins of the high catalytic activity of nanoporous gold. *Nat. Mater.* **11**, 775 (2012).
76. E-J. Gwak and J-Y. Kim: Weakened flexural strength of nanocrystalline nanoporous gold by grain refinement. *Nano Lett.* **16**, 2497 (2016).
77. L.H. Qian and M.W. Chen: Ultrafine nanoporous gold by low-temperature dealloying and kinetics of nanopore formation. *Appl. Phys. Lett.* **91**, 083105 (2007).
78. O.V. Shulga, K. Jefferson, A.R. Khan, V.T. D’Souza, J. Liu, A.V. Demchenko, and K.J. Stine: Preparation and characterization of porous gold and its application as a platform for immobilization of acetylcholine esterase. *Chem. Mater.* **19**, 3902 (2007).
79. J. Snyder, K. Livi, and J. Erlebacher: Dealloying silver/gold alloys in neutral silver nitrate solution: Porosity evolution, surface composition, and surface oxides. *J. Electrochem. Soc.* **155**, C464 (2008).
80. Z. Zhang, Y. Wang, Z. Qi, W. Zhang, J. Qin, and J. Frenzel: Generalized fabrication of nanoporous metals (Au, Pd, Pt, Ag, and Cu) through chemical dealloying. *J. Phys. Chem. C* **113**, 12629 (2009).
81. E. Detsi, Z. Vukovic, S. Punzhin, P.M. Bronsveld, P.R. Onck, and J.T.M.D. Hosson: Fine-tuning the feature size of nanoporous silver. *CrystEngComm* **14**, 5402 (2012).
82. H. Qiu, Z. Zhang, X. Huang, and Y. Qu: Dealloying Ag–Al alloy to prepare nanoporous silver as a substrate for surface-enhanced raman scattering: Effects of structural evolution and surface modification. *ChemPhysChem* **12**, 2118 (2011).
83. X. Wang, Z. Qi, C. Zhao, W. Wang, and Z. Zhang: Influence of alloy composition and dealloying solution on the formation and microstructure of monolithic nanoporous silver through chemical dealloying of Al–Ag alloys. *J. Phys. Chem. C* **113**, 13139 (2009).
84. C. Zhang, J. Sun, J. Xu, X. Wang, H. Ji, C. Zhao, and Z. Zhang: Formation and microstructure of nanoporous silver by dealloying rapidly solidified Zn–Ag alloys. *Electrochim. Acta* **63**, 302 (2012).
85. D.V. Pugh, A. Dursun, and S.G. Corcoran: Formation of nanoporous platinum by selective dissolution of Cu from Cu<sub>0.75</sub>Pt<sub>0.25</sub>. *J. Mater. Res.* **18**, 216 (2003).
86. Z. Dan, F. Qin, T. Wada, S-i. Yamaura, G. Xie, Y. Sugawara, I. Muto, A. Makino, and N. Hara: Nanoporous palladium fabricated from an amorphous Pd<sub>42.5</sub>Cu<sub>30</sub>Ni<sub>7.5</sub>P<sub>20</sub> precursor and its ethanol electro-oxidation performance. *Electrochim. Acta* **108**, 512 (2013).
87. M. Hakamada and M. Mabuchi: Fabrication of nanoporous palladium by dealloying and its thermal coarsening. *J. Alloys Compd.* **479**, 326 (2009).
88. M. Hakamada, H. Nakano, T. Furukawa, M. Takahashi, and M. Mabuchi: Hydrogen storage properties of nanoporous palladium fabricated by dealloying. *J. Phys. Chem. C* **114**, 868 (2010).
89. W. Li, H. Ma, L. Huang, and Y. Ding: Well-defined nanoporous palladium for electrochemical reductive dechlorination. *Phys. Chem. Chem. Phys.* **13**, 5565 (2011).
90. L-Y. Chen, J-S. Yu, T. Fujita, and M-W. Chen: Nanoporous copper with tunable nanoporosity for SERS applications. *Adv. Funct. Mater.* **19**, 1221 (2009).
91. J. Hayes, A. Hodge, J. Biener, A. Hamza, and K. Sieradzki: Monolithic nanoporous copper by dealloying Mn–Cu. *J. Mater. Res.* **21**, 2611 (2006).
92. H-B. Lu, Y. Li, and F-H. Wang: Synthesis of porous copper from nanocrystalline two-phase Cu–Zr film by dealloying. *Scr. Mater.* **56**, 165 (2007).
93. Z. Qi, C. Zhao, X. Wang, J. Lin, W. Shao, Z. Zhang, and X. Bian: Formation and characterization of monolithic nanoporous copper by chemical dealloying of Al–Cu alloys. *J. Phys. Chem. C* **113**, 6694 (2009).

94. C. Zhao, Z. Qi, X. Wang, and Z. Zhang: Fabrication and characterization of monolithic nanoporous copper through chemical dealloying of Mg–Cu alloys. *Corros. Sci.* **51**, 2120 (2009).
95. Z. Dan, F. Qin, Y. Sugawara, I. Muto, and N. Hara: Bimodal nanoporous nickel prepared by dealloying Ni<sub>38</sub>Mn<sub>62</sub> alloys. *Intermetallics* **31**, 157 (2012).
96. M. Hakamada and M. Mabuchi: Nanoporous nickel fabricated by dealloying of rolled Ni–Mn sheet. *Procedia Eng.* **81**, 2159 (2014).
97. H.J. Qiu, J.L. Kang, P. Liu, A. Hirata, T. Fujita, and M.W. Chen: Fabrication of large-scale nanoporous nickel with a tunable pore size for energy storage. *J. Power Sources* **247**, 896 (2014).
98. L. Sun, C-L. Chien, and P.C. Searson: Fabrication of nanoporous nickel by electrochemical dealloying. *Chem. Mater.* **16**, 3125 (2004).
99. S.K. Gordeev, S.A. Kukushkin, A.V. Osipov, and Y.V. Pavlov: Self-organization in the formation of a nanoporous carbon material. *Phys. Solid State* **42**, 2314 (2000).